

# ***Ab-initio* studies on phonons of BaTiO<sub>3</sub> polytypes: pressure dependences with a hybrid functional**

Yu-Seong Seo and Jai Seok Ahn\*

*Department of Physics, Pusan National University, Busan 609-735, Republic of Korea*

We report our first principles investigations on phonons of three polytypes of BaTiO<sub>3</sub> (BTO): paraelectric (PE) cubic  $Pm-3m$  and two ferroelectric (FE) phases, tetragonal  $P4mm$  and rhombohedral  $R3m$ . We reviewed the phonon frequencies calculated by using various exchange-correlation functionals, including density functional theory, Hartree-Fock approximation, and their hybrids. By calculating the phonon modes as a function of pressure, we demonstrated that theoretical trajectories of pressure-sensitive modes of FE phases showed softening and converged to the modes of PE phase at pressure below 20 GPa. These results on FE phases can be interpreted as phonon-precursors for symmetry change from low- to high-symmetry and partly as a theoretical explanation for the pressure-induced mode-coupling behaviors of Sood *et al.* [Phys. Rev. B **51**, 8892 (1995)]. The pressure-induced stabilization of imaginary-frequency-modes was also demonstrated by calculating phonon modes for all the possible directions of phonon-propagation vectors. As pressure increases, the imaginary-frequency-mode of  $P4mm$  was transformed into a stable mode in an orderly sequence of  $R-X-Z-\Gamma$ .

\* Email: [jaisahn@pusan.ac.kr](mailto:jaisahn@pusan.ac.kr)

Fax: +82-51-513-7664 (Dept.)

## I. INTRODUCTION

Ferroelectric (FE) materials have been used for a wide range of modern technologies targeted for storages and motions, such as in memory device, electromotive transducers, and sensors for medical imaging [1, 2]. The two essential features of FE material, the electrostatic polarization for storage and the piezoelectricity for motions, are closely related to structures belonging to subgroups of non-centrosymmetric piezoelectric group [2]. The FE perovskite oxides, such as  $\text{Pb}(\text{Zr,Ti})\text{O}_3$  (PZT), have three phases, rhombohedral, tetragonal, and cubic. And ferroelectricity occurs at the two non-centrosymmetric phases, tetragonal and rhombohedral, which are connected with a morphotropic phase boundary (MPB) composed of monoclinic/orthorhombic phase [3-7]. The existence of intermediate phase has been understood to be indispensable for the large piezoelectricity and polarization rotation mechanism across the MPB, as explained by Fu and Cohen [8], such as in PZT or  $\text{Ba}(\text{Ti,Zr})\text{O}_{3-x}(\text{Ba,Ca})\text{TiO}_3$ , (BTZ- $x$ BCT) [7, 9]. More recently, the evidences for local structures have been reported in relaxor-ferroelectrics, such as BTZ- $x$ BCT [10-12]. Neutron pair-distribution-function analysis provided notable local structural features departing from the given average crystallographic structures, such as local Ti distortions toward  $\langle 111 \rangle$ , trigonal 3:3 Ti-O length distribution, and single bond-length in Zr-O in BTZ- $x$ BCT [10, 11]. The Raman spectroscopy on BTZ/BTZ- $x$ BCT also showed rich interplay, between long-range average structure and short-range local orders, as a function of pressure [12, 13]. The phonon-interference effect in the pressure-dependent Raman spectra of  $\text{BaTiO}_3$  (BTO) was explained with coupled-phonon interaction of three  $A_1$  modes of tetragonal phase [14]. The off-center displacements of Ti ions in the cubic phase of BTO were found from NMR experiments [15].

FE BTO has been investigated using numerous first-principles methods [16-24]. King-Smith and Vanderbilt correctly predicted the symmetry of ground-state structure as rhombohedral [16]. In Zhong *et al.*'s pressure-temperature phase diagram, the sequence of

low temperature phases were obtained as rhombohedral, orthorhombic, tetragonal, and cubic, in increasing temperature [21]. Wu *et al.* obtained phonon frequencies of rhombohedral phase under a “negative fictitious pressure” to constrain the cell volume to be that of the experiment [23]. Pressure-dependence of BTO, however, has been rarely studied with first-principle methods until now, except for the recent report on tetragonal phase with local density approximation (LDA): Duan *et al.* studied the pressure effects on ferroelectricity and piezoelectricity of tetragonal BTO [24]. In this manuscript, we describe the structures and phonons of BTO polymorphs using the first-principles methods in two directions. In the first part, we compare the phonons of three polymorphs of BTO, paraelectric cubic and two FE phases, tetragonal and rhombohedral, calculated by using various exchange-correlation functionals including the hybrid methods. And in the second part, we discuss the pressure dependences of phonon modes calculated for phonon-propagation vectors at high-symmetry directions of three BTO polytypes.

## II. COMPUTATIONAL DETAILS

First-principles calculations were performed using the CRYSTAL09 code [25]. We used basis sets (BS) composed of Gaussian type orbitals. To describe heavy elements, such as barium and titanium, the Hay-Wadt effective core potentials with small-cores were adopted for BS's. Ba ( $5s/5p/6s$ ) and Ti ( $3s/3p/4s/3d$ ) electrons were considered as valence electrons for self-consistent calculations [26]. Thus, computational time could be minimized within our computational resources. For oxygen atom, full electron BS, O-411d11G, was used [27]. The reciprocal space integration was approximated by sampling the Brillouin zone with  $6\times 6\times 6$  mesh of Monkhorst-Pack scheme. The self-consistent cycles were repeated until a

convergence is reached within a tolerance of  $10^{-10}$  Ha ( $\sim 3 \times 10^{-9}$  eV) of total energy difference.

We compared ground state configurations calculated with a number of different exchange-correlation functionals among density functional theory (DFT), Hartree-Fock (HF) approximation, and their hybrids. This comparison allowed us to select the exchange-correlation functional, which describes well the lattice structural and electronic properties of three different structures of BTO. For DFT, local density approximation (LDA) and generalized gradient approximations, GGA [28] and PWGGA [29], were used. We applied three functional forms for hybrid methods for the more accurate band gap: B3LYP [25], B3PW [30], and PBE0 [31]. The B3LYP has a Becke's three parameter hybrid functional form [30], which includes HF exchange and the non-local correlation by Lee, Yang, and Parr [32], with  $A = 0.2$ ,  $B = 0.9$ , and  $C = 0.81$ :

$$E_{xc} = (1 - A) \cdot (E_x^{LDA} + B \cdot E_x^{Becke}) + A \cdot E_x^{HF} + (1 - C) \cdot E_c^{VWN} + C \cdot E_c^{LYP}, \quad (1)$$

where  $E_x^{LDA}$  and  $E_c^{VWN}$  are LDA exchange and Vosko-Wilk-Nusair correlation [33], which fits the Ceperley-Alder data for electron gas [34]. Similarly, The B3PW hybrid functional uses PWGGA,  $E_c^{PWGGA}$ , as a non-local correlation instead of  $E_c^{LYP}$  in B3LYP shown with Eq. (1). And the PBE0 is a parameter-free hybrid functional, which uses PBE (GGA) exchange-correlation mixed with 25% of HF exchange.

The equilibrium geometries were found by optimizing the lattice constants and fractional displacements of basis atoms for cubic ( $Pm-3m$ ), tetragonal ( $P4mm$ ), and rhombohedral ( $R3m$ ) structures of BTO: structural relaxations were repeated until the norm of total forces becomes less than  $3 \times 10^{-5}$  Ha/Bohr ( $\approx 1.5 \times 10^{-3}$  eV/Å). Phonon modes were calculated by using a frozen phonon method implemented in the CRYSTAL09 code. The

phonon dispersions were calculated by using a supercell method: a  $2 \times 2 \times 2$  supercell, that is consisting of 40 atoms, was assumed for each one of cubic, tetragonal, and rhombohedral (i.e.,  $2 \times 2 \times 1$  in hexagonal setting) structures. To get LO/TO splitting of zone-center phonon by non-analytic correction, which is due to long range electrostatic interactions in polar materials, electronic dielectric constants and Born effective charges were also calculated. The high frequency (optical) dielectric constants were calculated with the finite field perturbation method: the effect of “sawtooth” electric potential applied in supercell was evaluated numerically. For tetragonal or rhombohedral (in hexagonal setting) case, the anisotropic dielectric constants,  $\epsilon_{a,\infty}$  and  $\epsilon_{c,\infty}$ , were determined by applying an electric field through the long axes of supercells, taken along crystallographic  $a$  and  $c$  directions, respectively. The Born effective charges were evaluated through the Berry phase approach [35].

### III. RESULTS AND DISCUSSION

The results calculated for the relaxed geometries of three phases of  $\text{BaTiO}_3$  are summarized in Table 1. The cell volumes of the three structures calculated with the B3PW hybrid functional overestimate the LDA results, but give better estimations for experimental volumes. However, the tetragonality factor,  $c/a \approx 1.046$ , of  $P4mm$ , calculated by using the B3PW functional overestimates the results from LDA ( $\sim 1.011$ ) or the experimental value ( $\sim 1.010$ ). These generic behaviors regarding the lattice parameters, the successful reproduction of the cell volumes and the super-tetragonality (of  $P4mm$ ), can be attributed to the non-local exchange-correlation functional embedded within the GGA-derived hybrid functionals, which is well-known for accurate predictions for the cell volumes. The electronic dielectric constants  $\epsilon_\infty$  calculated for three phases underestimate the LDA predictions or the experimental values. The Born effective charges (BEC’s) were calculated by using the Berry

phase method for the fully relaxed geometries. Among the calculated tensor components of BEC's, most of them are slightly smaller than LDA results for all phases, except for  $\mathbf{Z}_{zz}^*$  (Ba) of tetragonal;  $\mathbf{Z}_{xz}^*(0)$  and  $\mathbf{Z}_{yz}^*(0)$  of rhombohedral. The underestimations of  $\epsilon_\infty$ 's and the  $\mathbf{Z}^*$ 's need to be analyzed concurrently, because they influence on the LO phonon modes in different ways, as will be discussed below.

The BEC's are dynamic charges useful for calculating the so-called LO-TO splitting through a non-analytical correction in polar materials like BaTiO<sub>3</sub>. In the long-wavelength limit, the dynamical matrix  $D_{\alpha,\beta}(\mathbf{k}; \mu\nu)$  of a polar crystal can be written as the sum of analytical  $D_{\alpha,\beta}^{(0)}(\mathbf{k}; \mu\nu)$  and non-analytical contributions [37], such as

$$D_{\alpha,\beta}(\mathbf{k}; \mu\nu) = D_{\alpha,\beta}^{(0)}(\mathbf{k}; \mu\nu) + \frac{4\pi e^2}{V\epsilon_\infty\sqrt{M_\mu M_\nu}} \frac{[\mathbf{k}\cdot\mathbf{Z}^*(\mu)]_\alpha[\mathbf{k}\cdot\mathbf{Z}^*(\nu)]_\beta}{|\mathbf{k}|^2}, \quad (2)$$

where  $D_{\alpha,\beta}^{(0)}(\mathbf{k}; \mu\nu)$  is the dynamical matrix derived with the direct method from the Hellmann-Feynman forces. In Eq. (2),  $\mathbf{k}$  is the wave vector;  $V$  is the volume of the primitive cell;  $M_\mu$  and  $\mathbf{Z}^*(\mu)$  are atomic masses and the BEC tensor of atom indexed with  $\mu$ . The non-analytic contributions are proportional to the squares of  $\mathbf{Z}^*$ 's but inverse-proportional to  $\epsilon_\infty$ 's. Therefore, the effects from the small underestimations of the BEC's are clearly overwhelmed by the (relatively) larger effect by the underestimations of  $\epsilon_\infty$ 's: i.e., the LO-TO splitting is dominated by the differences in  $\epsilon_\infty$ 's rather by the  $\mathbf{Z}^*$ 's.

## 1. Optical phonon modes at ambient pressure

In the cubic perovskite structure of BaTiO<sub>3</sub> with  $Pm-3m$  symmetry, i.e., with space group (SG) No. 221, there are 12 optical modes at  $\Gamma$ -point (i.e., at zone-center): three triply degenerate modes of  $F_{1u}$  and one triply degenerate silent mode of  $F_{2u}$  symmetry, with  $\Gamma_{\text{optic}} = 3F_{1u} +$

$F_{2u}$  as its irreducible representation at  $\Gamma$ -point. In the tetragonal  $\text{BaTiO}_3$  with  $P4mm$  symmetry (SG No. 99), each of the  $F_{1u}$  modes splits into a nondegenerate  $A_1$  mode and a doubly degenerate  $E$  mode, and the  $F_{2u}$  mode splits into  $E$  and  $B_1$  modes: i.e.,  $\Gamma_{\text{optic}} = 3A_1 + B_1 + 4E$ , where the  $E$  and  $A_1$  modes are both infrared (IR) and Raman active, while the  $B_1$  is a Raman only mode. Similarly in the rhombohedral  $\text{BaTiO}_3$  with  $R3m$  symmetry (SG No. 160), the  $F_{1u}$  splits into  $A_1$  &  $E$  and the  $F_{2u}$  into  $A_2$  &  $E$ ;  $\Gamma_{\text{optic}} = 3A_1 + A_2 + 4E$ , with the  $A_2$  being a Raman only mode [38].

Zone-center optical phonon modes calculated by using the B3PW functional are summarized in Table 2. Symmetries and frequencies of phonon modes for all the three phases were obtained. The LO-TO splitting is calculated by applying the non-analytical corrections along (100) directions. In agreement with the previous LDA results [20, 36], we obtained non-stable modes with imaginary frequencies, i.e., soft modes signifying structural instability, for cubic and tetragonal phases of  $\text{BaTiO}_3$ ; real frequencies were calculated for all the modes in the rhombohedral phase. Mode frequencies calculated by using the B3PW functional are in average comparable to the LDA results [20, 36], except a few out-of-ordered TO modes around  $\sim 300 \text{ cm}^{-1}$ . Note that the compared LDA results for tetragonal and rhombohedral structures were calculated by constraining the cell volume to experimental value [36]; our present results were obtained from the fully relaxed geometry including the cell volume without any assumption.

Zone-center optical phonon modes were also calculated for three BTO phases by using various exchange-correlation functionals, such as HF, LDA, PWGGA, PBE(GGA), B3LYP, B3PW, and PBE0. The results are plotted in Fig. 1: closed symbols represent TO modes; open symbols for LO modes. Firstly, the results from GGA are indistinguishable from PWGGA results. The three hybrid functionals provide similar results: the results from B3PW fully agrees with the PBE0 results; the B3LYP provide slightly lower (in  $Pm-3m$ ) or slightly

higher (in  $P4mm/R3m$ ) frequencies. The results from LDA or from HF are rather off from the results of other functionals: the LDA gives out-of-ordered TO modes near  $300\text{ cm}^{-1}$  for both  $P4mm$  and  $R3m$ ; the HF provides no soft-modes for  $P4mm$ , while all other functionals do. In  $Pm-3m$  phase, shown in Fig. 1(a), phonon modes do not vary much irrespective of the functional choices.

## 2. Pressure dependence of phonon modes and structural instability

If the phonon modes are calculated as a function of pressure, one can see the evolutions and interplays of modes. In addition, one can understand more clearly that the connections between the irreducible representations of each structure. The phonon modes were calculated for fully relaxed geometries under applied hydrostatic pressures; pressures ranged from -10 to 20 GPa. We chose the B3PW hybrid functional for pressure-dependent calculations, because it reproduces the experimental cell volumes and energy gaps for the three BTO phases. The results (by using the B3PW functional) are shown in Fig. 2: the eight modes for  $P4mm$  (in Fig. 2(a)) and  $R3m$  (in Fig. 2(b)); the four modes for  $Pm-3m$  (shown with dashed lines on both panels). The data points at  $P = 0$  reproduce the phonon modes tabulated in Table 2. (Note that the LO-TO splitting was not considered here.) As pressure increases, most modes show blue-shifting behaviors due to the mode Grüneissen effect [39]. The trajectories of modes converged to one of the four modes of  $Pm-3m$ , three  $F_{1u}$ 's and one  $F_{2u}$ , by applying positive pressures. The  $E$  and  $A_1$  were merged into  $F_{1u}$ ; the  $E$  and  $B_1$  into  $F_{2u}$ , in  $P4mm$ . Similarly, the  $E$  and  $A_1$  were merged into  $F_{1u}$ ; the  $E$  and  $A_2$  into  $F_{2u}$ , in  $R3m$ . The most exotic behavior is found from the pressure-trajectories of two modes,  $142i$  ( $E$ ) and  $397$  ( $A_1$ ) of  $P4mm$ ;  $267$  ( $E$ ) and  $338$  ( $A_1$ ) of  $R3m$ , tabulated in Table 2 (calculated at  $P = 0$ ). The trajectories of the two modes were merged into the lowest  $F_{1u}$  lines by applying pressures up to at  $\sim 18$  GPa. As pressure increases, the unstable mode with imaginary frequency becomes a real-frequency

mode by applying pressure of  $\sim 20$  GPa for  $P4mm$ ;  $\sim 16$  GPa for  $Pm-3m$ . In  $R3m$ , on the other hand, two modes ( $E$  and  $A_1$ ) become soft, and eventually merge to the lowest  $F_{1u}$  lines.

The calculated pressure-dependence of phonon modes of  $P4mm$  can provide the long-awaited explanation based on the first-principles regarding the pressure-induced phonon-coupling behaviors reported years ago by Sood *et al.* [14]. According to Sood *et al.*, three  $A_1(\text{TO})$  modes showed anomalous behaviors as a function of pressure, for  $P = 0-4$  GPa: (i) non-monotonic pressure-dependences at  $\sim 2$  GPa, (ii) asymmetries in the line shapes, (iii) interference effects, *etc.* Those behaviors were explained with the existence of coupled-mode interaction involving only phonon together with the structural transition from tetragonal to cubic occurring at 2.2 GPa. Our results, shown in Fig. 2(a), reproduce only some of their observations: two  $A_1$  modes showed (counter-intuitive) softening behavior as a function of pressure, and the pressure-rates of the modes were non-monotonic, however, no peculiarity was found at  $\sim 2$  GPa. Such behaviors of the two  $A_1$  modes with increasing pressures, however, can be interpreted as precursors of symmetry change from low- to high-symmetry: the two  $A_1$  modes (with two  $E$  modes) are merged to the  $F_{1u}$  modes of cubic phase, as indicated in the compared results on the cubic phase,  $Pm-3m$ , indicated with dashed lines in Fig. 2(a). In addition, any non-linearity, which may be required for the mode-coupling model by Sood *et al.*, is beyond the capability of our calculation, because our first-principles calculation is limited to the harmonic approximation for phonon modes.

So far, we discussed the phonon modes at  $\Gamma$ -point. To find out the full extent of structural stability, one needs to examine the phonon modes of all the possible directions of phonon-propagation vectors. The optical phonon modes were calculated for the propagation vectors pointing at high-symmetry points of the Brillouin zone (BZ): the vectors were at  $\Gamma$  (000),  $X$  (010),  $Z$  (001),  $M$  (110),  $R$  (011), and  $A$  (111) for  $P4mm$ ; at  $\Gamma$  (000),  $X$  (001),  $M$  (011), and  $R$  (111) for both  $R3m$  and  $Pm-3m$ . The above vectors are compatible with the  $2 \times 2 \times 2$

supercells used for dispersion calculations at each of cubic, tetragonal, and rhombohedral structures, i.e., the calculated phonon frequencies at these points are exact within numerical errors. Note that some characters for BZ points in one structure deliver different meanings in another structure, as will be discussed below: for example, the  $R$  point in  $P4mm$ , i.e. representing (011) point, corresponds to the  $M$  point in  $R3m$  or  $Pm-3m$ ; the  $A$  point for (111) in  $P4mm$  to the  $R$  point in  $R3m$  or  $Pm-3m$ .

To check the stability of structures of  $Pm-3m$ ,  $P4mm$ , and  $R3m$  symmetries at ambient pressures, the optical phonon modes were calculated for phonon-propagation vectors at high-symmetry points of the BZ. Firstly, the imaginary phonon modes of  $P4mm$ , shown in Fig. 3(a), are clearly contrasted from the non-imaginary modes of  $R3m$ , shown in Fig. 3(b). The results for  $P4mm$  showed the imaginary modes at  $\Gamma$ ,  $X$ ,  $Z$ , and  $R$ , while not at  $M$  or  $A$  points: it means the structure is unstable with respect to phonon perturbations at four out of six high-symmetry points under consideration. The  $Pm-3m$  structure of  $BaTiO_3$  was also found to be unstable from the calculated imaginary frequencies at  $\Gamma$ ,  $X$ , and  $M$ , except at  $R$  (not shown here). On the other hand, the  $R3m$  has no imaginary frequencies for all high-symmetry points, which means that the structure is stable. One may have predicted the stability of the  $R3m$  from the findings of real-frequency-modes at  $A$  point in  $P4mm$  and  $R$  point in  $Pm-3m$ , both correspond to the trigonal perturbations along (111) directions.

The pressure-dependence of the optical phonon modes were calculated also for the high-symmetry points. Figure 4 summarizes the results for  $P4mm$  tetragonal and  $Pm-3m$  cubic. The results for  $P4mm$  are intriguing if compared with the results at  $P = 0$ . Originally, at  $P = 0$ , the imaginary frequencies were found at the four directions,  $\Gamma$ ,  $X$ ,  $Z$ , and  $R$ , of  $P4mm$ , as shown in Fig. 3(a). The number of unstable modes decreases to two, at  $\Gamma$  and  $Z$  directions, at  $P = 10$  GPa shown in Fig. 4(a), and becomes none at  $P = 18$  GPa in Fig. 4(b). From these findings and from the movement of modes, we can analyze that the soft-mode-instability of

$P4mm$  is removed sequentially in the order of  $R-X-Z-\Gamma$  as pressure increases. The results for  $P4mm$  can be compared with the  $Pm-3m$  cases, shown in Fig. 4(c) for  $P = 10$  GPa and in Fig. 4(d) for  $P = 18$  GPa. The unstable modes were found at  $\Gamma$ ,  $X$ , and  $M$  directions at  $P = 0$ . All the soft modes moved upward at  $P = 10$  GPa, and became stable modes at  $P = 18$  GPa. Therefore, the removal sequence for the soft-mode-instability of  $Pm-3m$  is analyzed to be in the order of  $M-X-\Gamma$  as a function of pressure.

#### IV. CONCLUSION

We calculated phonon modes of three polytypes of  $\text{BaTiO}_3$ ,  $Pm-3m$ ,  $P4mm$ , and  $R3m$ , with *ab-initio* calculations using DFT, HF, and hybrid functionals. Zone-center optical phonon modes calculated from the fully relaxed geometries without any assumption using seven different exchange-correlation functionals were compared the previous LDA results obtained by constraining the cell volume. Pressure-induced phonon-trajectories showed the softening and convergence of pressure-sensitive modes of FE phases into the modes of PE phase at pressure below  $\sim 20$  GPa. Phonon modes for the phonon-propagation vectors at high-symmetry directions demonstrate the pressure-induced stabilizing sequence of imaginary-frequency modes.

#### ACKNOWLEDGMENTS

This work is supported by the National Research Foundation of Korea (NRF) grant funded by the Ministry of Education, Science and Technology (MEST), No. 2012006641. The computation is supported by the Korea Institute of Science and Technology Information (KISTI) Supercomputing Center through contract No. KSC-2012-C2-36.

## REFERENCES

- [1] D. C. Hill and H. L. Tuller, *Ceramic Sensors: Theory and Practice*, edited by L. M. Levinson (Marcel Dekker, New York, 1988), pp. 265–374.
- [2] G. H. Haertling, *J. Am. Ceram. Soc.* **82**, 797 (1999).
- [3] G. Shirane, K. Suzuki, and A. Takeda, *J. Phys. Soc. Jpn.* **7**, 12 (1952).
- [4] B. Jaffe, R. S. Roth, and S. Marzullo, *J. Appl. Phys.* **25**, 809 (1954).
- [5] B. Jaffe, W. R. Cook, and H. Jaffe, *Piezoelectric Ceramics* (Academic, New York, 1971).
- [6] B. Noheda, J. A. Gonzalo, L. E. Cross, R. Guo, S.-E. Park, D. E. Cox, and G. Shirane, *Phys. Rev. B* **61**, 8687 (2000).
- [7] D. Damjanovic, *Appl. Phys. Lett.* **97**, 062906 (2010).
- [8] H. Fu and R. E. Cohen, *Nature* **403**, 281 (2000).
- [9] W. Liu and X. Ren, *Phys. Rev. Lett.* **103**, 257602 (2009).
- [10] I.-K. Jeong, C. Y. Park, J. S. Ahn, S. Park, and D. J. Kim, *Phys. Rev. B* **81**, 214119 (2010).
- [11] I.-K. Jeong and J. S. Ahn, *Appl. Phys. Lett.* **101**, 242901 (2012).
- [12] Y.-S. Seo, J. S. Ahn, and I.-K. Jeong, *J. Korean Phys. Soc.* **62**, 749 (2013).
- [13] J. Kreisel, P. Bouvier, M. Maglione, B. Dkhil, and A. Simon, *Phys. Rev. B* **69**, 092104 (2004).
- [14] A. K. Sood, N. Vhandrabhas, D. V. S. Muthu, and A. Jayaraman, *Phys. Rev. B* **51**, 8892 (1995).
- [15] B. Zalar, V. V. Laguta, and R. Blinc, *Phys. Rev. Lett.* **90**, 037601 (2003); R. Pirc and R. Blinc, *Phys. Rev. B* **70**, 134107 (2004).
- [16] R. D. King-Smith and D. Vanderbilt, *Phys. Rev. B* **49**, 5828 (1994).
- [17] Ph. Ghosez, E. Cockayne, U. V. Waghmare, and K. M. Rabe, *Phys. Rev. B* **60**, 836 (1999).

- [18] D. I. Bilc, R. Orlando, R. Shaltaf, G.-M. Rignanese, J. Íñiguez, and Ph. Ghosez, *Phys. Rev. B* **77**, 165107 (2008).
- [19] J. J. Wang, F. Y. Meng, X. Q. Ma, M. X. Xu, and L. Q. Chen, *J. Appl. Phys.* **108**, 034107 (2010).
- [20] R. A. Evarestov and A. V. Bandura, *J. Comp. Chem.* **33**, 1123 (2012).
- [21] W. Zhong, D. Vanderbilt, and K. M. Rabe, *Phys. Rev. B* **52**, 6301 (1995).
- [22] Q. Zhang, T. Cagin, and W. A. Goddard III, *Proc. Nat. Acad. Sci.* **103**, 14695 (2006).
- [23] X. Wu, D. Vanderbilt, and D. R. Hamann, *Phys. Rev. B* **72**, 035105 (2005).
- [24] Y. Duan, G. Tang, C. Chen, T. Lu, and Z. Wu, *Phys. Rev. B* **85**, 054108 (2012).
- [25] R. Dovesi, R. Orlando, B. Civalleri, C. Roetti, V. R. Saunders, and C. M. Zicovich-Wilson, *Z. Kristallogr.* **220**, 571 (2005); R. Dovesi, V. R. Saunders, C. Roetti, R. Orlando, C. M. Zicovich-Wilson, F. Pascale, B. Civalleri, K. Doll, N. M. Harrison, I. J. Bush, P. D'Arco, and M. Llunell, *CRYSTAL09 User's Manual* (University of Torino, Torino, 2009).
- [26] S. Piskunov, E. Heifets, R. I. Eglitis, and G. Borstel, *Comp. Mat. Sci.* **29**, 165 (2004).
- [27] L. Valenzano, F. J. Torres, K. Doll, F. Pascale, C. M. Zicovich-Wilson, and R. Dovesi, *Z. Phys. Chem.* **220**, 893 (2006).
- [28] J. P. Perdew, K. Burke, and M. Ernzerhof, *Phys. Rev. Lett.* **77**, 3865 (1996).
- [29] J. P. Perdew, J. A. Chevary, S. H. Vosko, K. A. Jackson, M. R. Pederson, D. J. Singh, and C. Fiolhais, *Phys. Rev. B* **46**, 6671 (1992).
- [30] A. D. Becke, *J. Chem. Phys.* **98**, 5648 (1993).
- [31] C. Adamo and V. Barone, *J. Chem. Phys.* **110**, 6158 (1999).
- [32] C. Lee, W. Yang, and R. G. Parr, *Phys. Rev. B* **37**, 785 (1988).
- [33] S. H. Vosko, L. Wilk, and M. Nusair, *Can. J. Phys.* **58**, 1200 (1980).
- [34] D. M. Ceperley and B. J. Alder, *Phys. Rev. Lett.* **45**, 566 (1980).

- [35] R. D. King-Smith and D. Vanderbilt, *Phys. Rev. B* **47**, 1651 (1993); D. Vanderbilt and R. D. King-Smith, *ibid.* **48**, 4442 (1993); R. Resta, *Rev. Mod. Phys.* **66**, 899 (1994).
- [36] P. Hermet, M. Veithen, and Ph. Ghosez, *J. Phys. Condens. Matter* **21**, 215901 (2009).
- [37] K. Parlinski, J. Łażewski, and Y. Kawazoe, *J. Phys. Chem. Sol.* **61**, 87 (2000).
- [38] C. J. Bradley and A. P. Cracknell, *The Mathematical Theory of Symmetry in Solids* (Clarendon, Oxford, 1972).
- [39] N. W. Ashcroft and N. D. Mermin, *Solid State Physics* (Saunders, Philadelphia, 1976), p. 493.

Table 1. Calculated lattice parameters (in Å), dielectric constants, and Born-effective-charge tensors ( $Z^*$  in  $|e|$ ) of the cubic, tetragonal, and rhombohedral phases of BaTiO<sub>3</sub>. Present hybrid calculations with B3PW are compared with LDA results.

	<b>Cubic</b>		<b>Tetragonal</b>		<b>Rhombohedral</b>	
	Present	LDA [20]	Present	LDA [36]	Present	LDA [36]
$a$	3.980	3.958	$a$ : 3.973 $c$ : 4.157	3.994 4.036	$a_R$ : 4.037 $\alpha$ : 89.724°	4.003 89.84°
$\epsilon_\infty$	4.94	6.32	$a$ : 4.61 $c$ : 4.12	6.48 5.84	4.59 4.10	6.16 5.73
Ba: $Z^*$	2.666	2.74	$xx$ : 2.638 $zz$ : 2.849	2.726 2.814	2.725 2.530	2.783 2.737
Ti:	7.027	7.30	$xx$ : 6.535 $zz$ : 5.005	7.044 5.971	6.134 4.918	6.608 5.765
O:	$xx$ : -5.601 $zz$ : -2.046	-5.80 -2.12	O <sub>1</sub> : $xx$ : -1.871 $zz$ : -4.068	-2.024 -4.836	O: $xx$ : -2.414 $xy$ : -0.933 $xz$ : 0.656 $yx$ : -0.933 $yy$ : -3.491 $yz$ : 1.136 $zx$ : 0.545 $zy$ : 0.944 $zz$ : -2.483	-2.562 -0.984 0.647 -0.984 -3.699 1.121 0.733 1.269 -2.834
			O <sub>2</sub> : $xx$ : -2.018 $yy$ : -5.283 $zz$ : -1.893	-2.149 -5.596 -1.974		

Table 2. Calculated frequencies ( $\text{cm}^{-1}$ ) of the zone-center phonon modes of the cubic, tetragonal, and rhombohedral phases of  $\text{BaTiO}_3$ . Present hybrid calculations with B3PW are compared with LDA results.

	Cubic		Tetragonal		Rhombohedral	
	Present	LDA [20]	Present	LDA [36]	Present	LDA [36]
TO			142i ( $E$ )	161i	177 ( $E$ )	163
			170 ( $A_1$ )	161	182 ( $A_1$ )	167
	236i ( $F_{1u}$ )	133i	179 ( $E$ )	167	267 ( $E$ )	210
	192 ( $F_{1u}$ )	193	298 ( $B_1$ )	287	299 ( $A_2$ )	277
	313 ( $F_{2u}$ )	296	317 ( $E$ )	284	318 ( $E$ )	293
	488 ( $F_{1u}$ )	483	397 ( $A_1$ )	302	338 ( $A_1$ )	259
			481 ( $E$ )	457	492 ( $E$ )	470
		599 ( $A_1$ )	507	567 ( $A_1$ )	512	
LO			173 ( $E$ )	162	188 ( $E$ )	174
			207 ( $A_1$ )	180	195 ( $A_1$ )	178
	182 ( $F_{1u}$ )	187	314 ( $E$ )	284	317 ( $E$ )	293
	481 ( $F_{1u}$ )	461	470 ( $E$ )	444	467 ( $E$ )	441
	720 ( $F_{1u}$ )	698	490 ( $A_1$ )	452	495 ( $A_1$ )	461
			713 ( $E$ )	641	733 ( $A_1$ )	687
			797 ( $A_1$ )	705	746 ( $E$ )	676

## Figure Captions

Fig. 1. Optical phonon modes at  $\Gamma$ -point calculated within different functionals for (a)  $Pm-3m$  cubic, (b)  $P4mm$  tetragonal, and (c)  $R3m$  rhombohedral phases of  $BaTiO_3$ . For  $Pm-3m$ :  $F_{1u}$  (●) and  $F_{2u}$  (●); For  $P4mm$ :  $E$  (●),  $A_1$  (●), and  $B_1$  (●); For  $R3m$ :  $E$  (●),  $A_1$  (●), and  $A_2$  (●). Open circles designate corresponding LO modes.

Fig. 2. Pressure dependences of optical phonon modes at  $\Gamma$ -point calculated for (a)  $P4mm$  and for (b)  $R3m$  phases of  $BaTiO_3$ . For  $P4mm$ :  $E$  (●),  $A_1$  (●), and  $B_1$  (●); For  $R3m$ :  $E$  (●),  $A_1$  (●), and  $A_2$  (●). Results for  $Pm-3m$  cubic phases are overlaid with dashed lines. The B3PW functional was used for calculations.

Fig. 3. Optical phonon modes calculated for phonon-propagation vectors at high-symmetry points of the BZ: of (a)  $P4mm$  tetragonal for vectors at  $\Gamma$ ,  $X$ ,  $Z$ ,  $M$ ,  $R$ , and  $A$ ; of (b)  $R3m$  rhombohedral for vectors at  $\Gamma$ ,  $X$ ,  $M$ , and  $R$ . Modes with imaginary frequencies are plotted below zero.

Fig. 4. Optical phonon modes calculated under hydrostatic pressures for phonon-propagation vectors at high-symmetry points of the BZ of  $P4mm$  tetragonal and  $Pm-3m$  cubic phases: (a) for  $P4mm$  at 10 GPa; (b) for  $P4mm$  at 18 GPa; (c) for  $Pm-3m$  at 10 GPa; (d) for  $Pm-3m$  at 18 GPa.

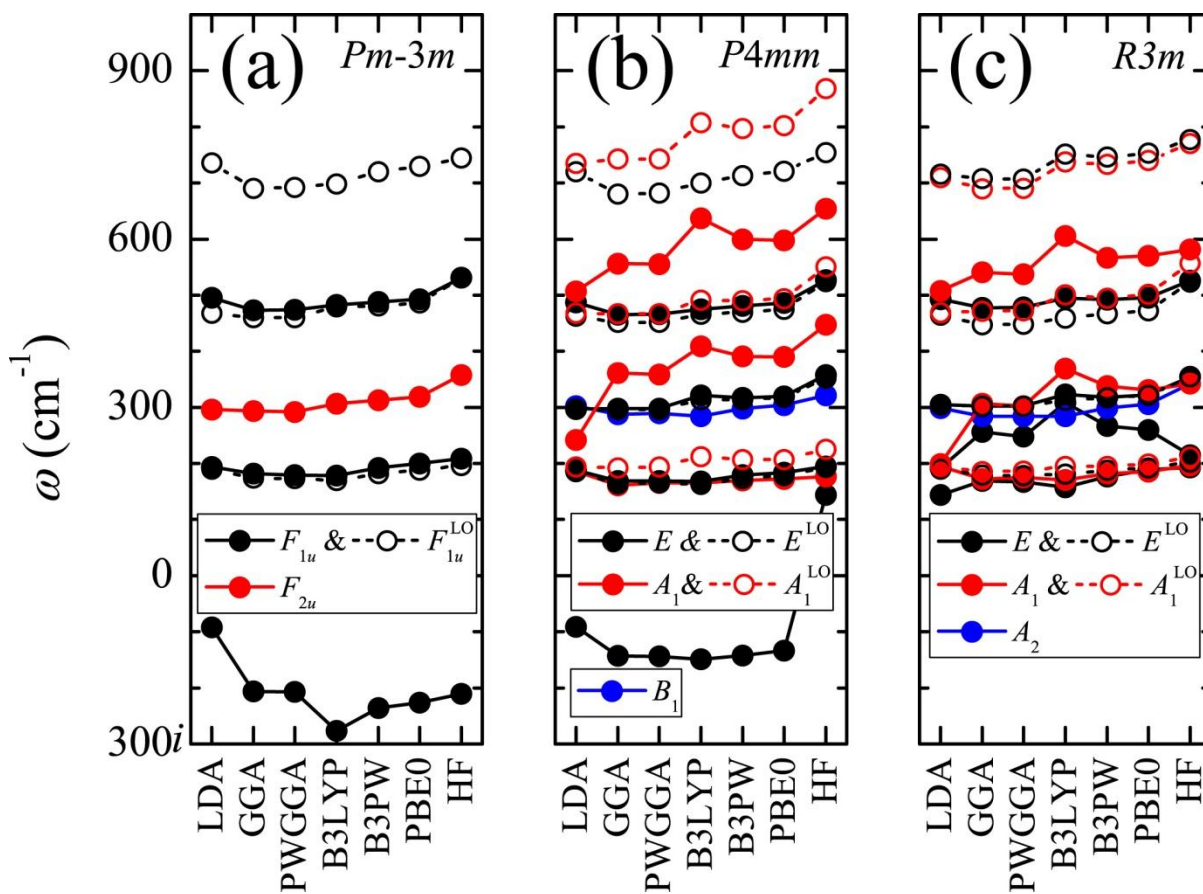


Fig. 1 of Seo and Ahn

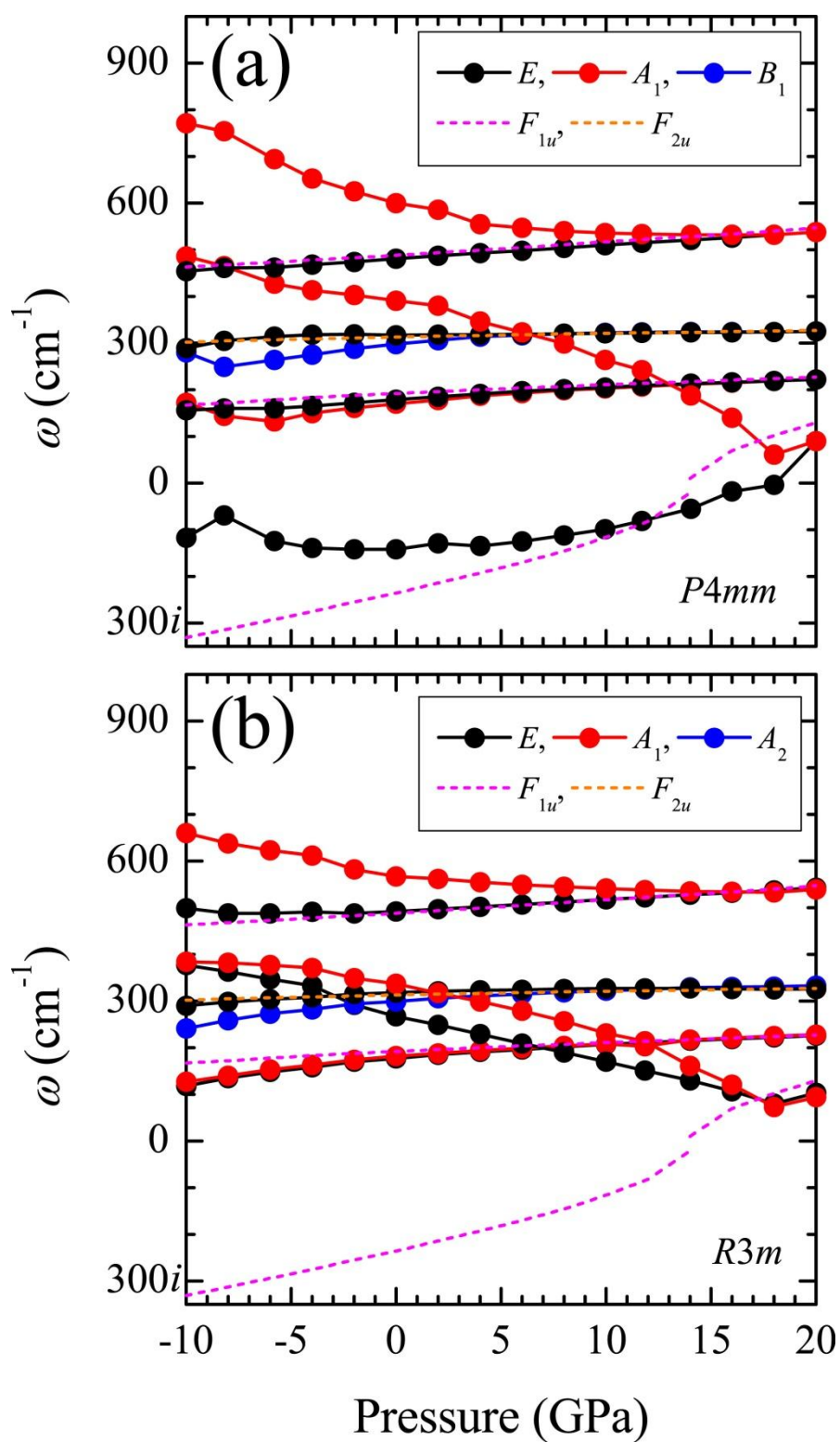


Fig. 2 of Seo and Ahn

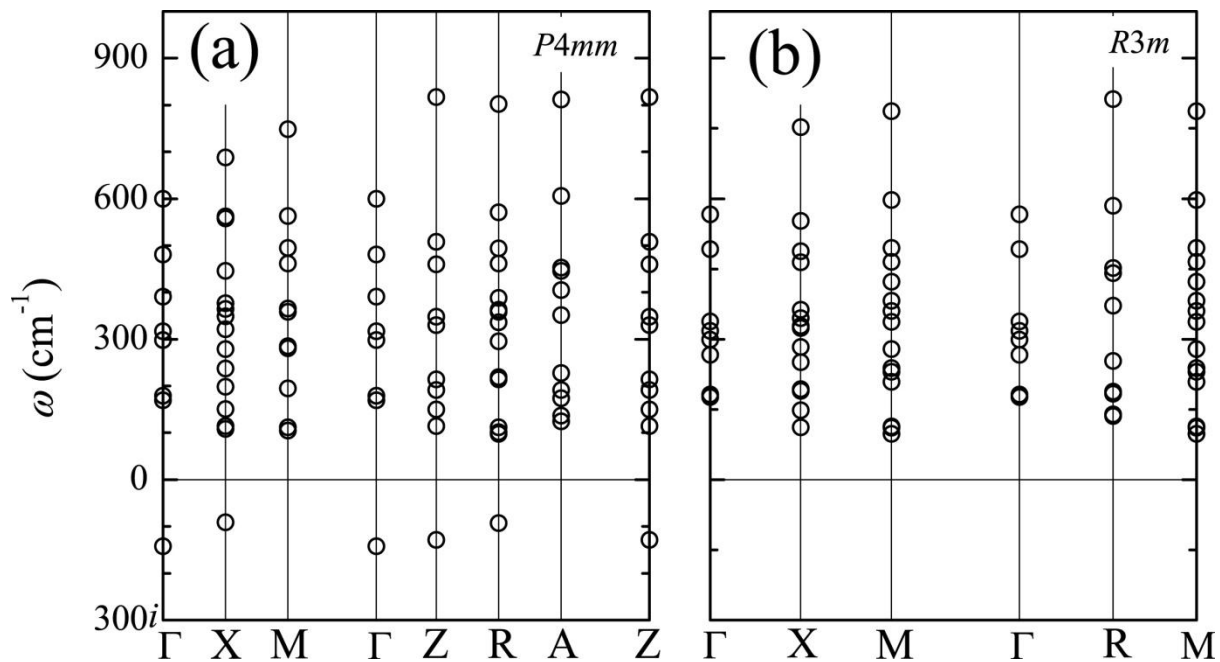


Fig. 3 of Seo and Ahn

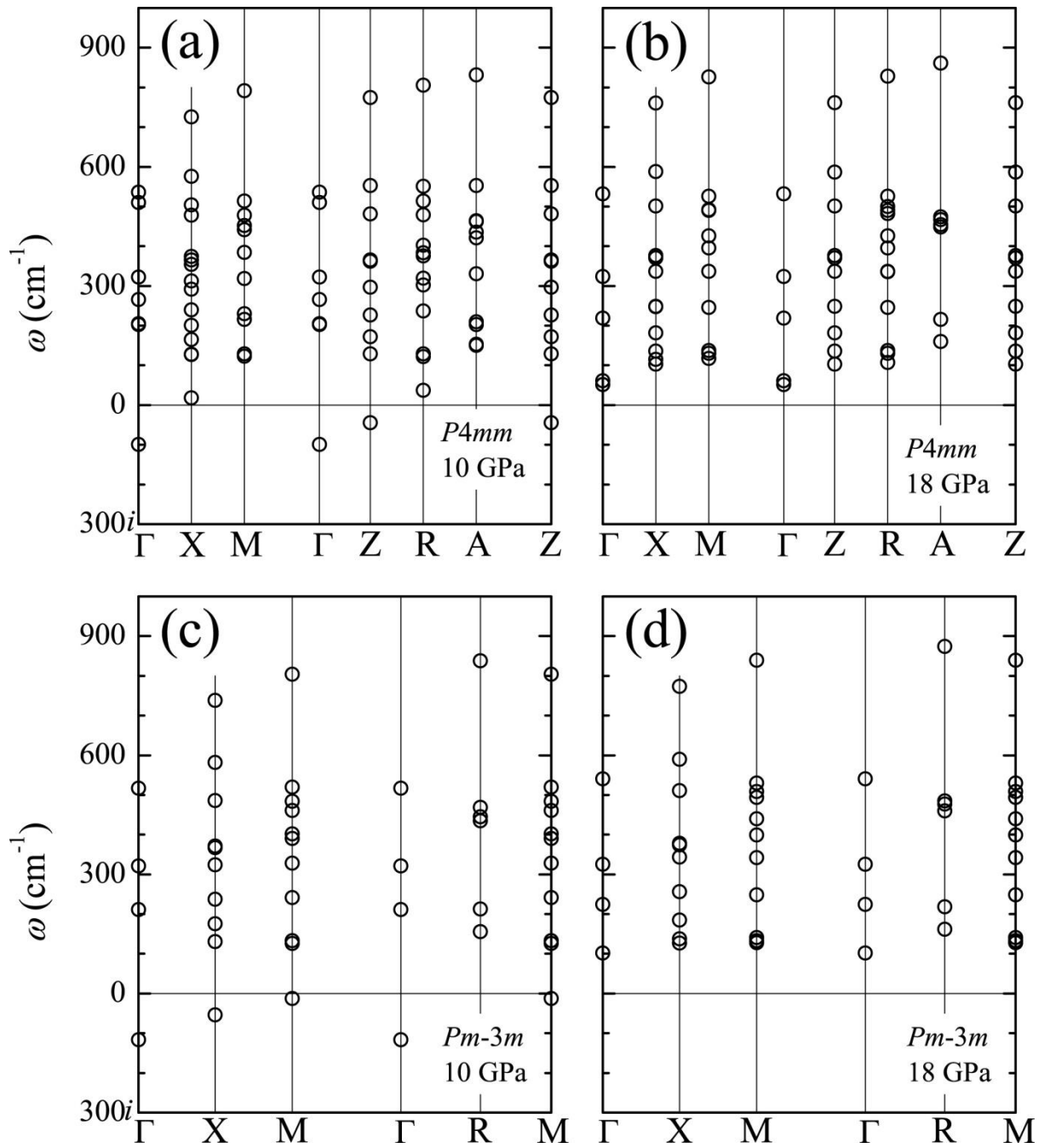


Fig. 4 of Seo and Ahn